metals

MDPI

Review

Engineering Heterogeneous Nucleation during Solidification of Multiphase Cast Alloys: An Overview

Simon N. Lekakh [1,*] and Jingjing Qing [2]

[1] Materials Science and Engineering Department, Missouri University of Science and Technology, Rolla, MO 65409, USA
[2] Manufacturing Engineering Department, Georgia Southern University, Statesboro, GA 30460, USA; jqing@georgiasouthern.edu
* Correspondence: lekakhs@mst.edu

Abstract: The theory of heterogeneous nucleation was initially developed as a part of condensed matter physics, and later it was used as an important engineering tool to design metallurgical processes. This success has led to wide applications of the theory in metallurgical practice. For example, engineering heterogeneous nucleation in ductile iron has been used to reduce shrinkage defects, suppress cementite formation, and modify the size and shape of microstructural constituencies. This demonstrates how theoretical knowledge could benefit industry practice. This overview aims to summarize the authors' published studies in co-authorship with colleagues and students, which covers different aspects of engineering heterogeneous nucleation in multiphase cast alloys. Several approaches for engineering heterogeneous nucleation using thermodynamic simulation as well as practical methods for improving efficiency of nucleation using the co-precipitation technique and a local transient melt supersaturation are suggested. Automated scanning electron microscopy/energy-dispersive X-ray (SEM/EDX) analysis and high-resolution transmission electron microscopy (TEM) were used to verify the simulation predictions. Practical examples of controlling microporosity shrinkage in cast irons with spheroidal graphite are presented to illustrate the power of engineering heterogenous nucleation.

Keywords: heterogeneous nucleation; solidification; structure modification; cast alloys; cast iron with spheroidal graphite; alloys with primary crystalline phase

check for updates

Citation: Lekakh, S.N.; Qing, J. Engineering Heterogeneous Nucleation during Solidification of Multiphase Cast Alloys: An Overview. *Metals* **2023**, *13*, 1154. https://doi.org/10.3390/met13071154

Academic Editor: Changming Fang

Received: 5 June 2023
Revised: 19 June 2023
Accepted: 20 June 2023
Published: 21 June 2023

Copyright: © 2023 by the authors. Licensee MDPI, Basel, Switzerland. This article is an open access article distributed under the terms and conditions of the Creative Commons Attribution (CC BY) license (https://creativecommons.org/licenses/by/4.0/).

1. Introduction of Engineering Heterogenous Nucleation in Multiphase Alloys

The theory of heterogeneous nucleation was initially developed by Gibbs, Turnbull and others as a part of condensed matter physics, and later it was used by Kurz, Stefanesku and others as an important engineering tool to design metallurgical processes. Multiphase alloys, which belong to eutectic systems, such as cast irons (*Fe*-C) and aluminum–silicon (*Al-Si*) alloys, are commonly used in the metal casting industry due to their good technological properties. For example, cast irons and *Al-Si* alloys with eutectic reactions have higher castability than alloys solidified in a single solid solution phase, such as steels (with austenite) or wrought *Al* alloys (with *α-Al*). The mechanical performance of multiphase alloys strongly depends on the microstructural dispersity and shape of the microconstituents in the microstructure. Refining the microstructure benefits most mechanical properties, and one popular approach to refining the microstructure is increasing the population of grains via promoting heterogeneous nucleation [1–3]. Therefore, controlling the microstructure in multicomponent alloys by enhancing heterogeneous nucleation is critically important for obtaining high-performance cast alloys. When compared to alloys in a single solid solution phase, commonly used multiphase alloys, for example cast irons, are not deformable and the shape of the primary phases is not intended to be changed during heat treatment. This overview of the authors' publications addresses modifying the microstructure in multiphase cast alloys during solidification.

Considering the size and number of structural units needed to nucleate in different types of cast alloys (Figure 1), the inoculation of grains in commercial multiphase alloys requires a significantly larger number of heterogeneous nuclei when compared to alloys solidified in a single phase [3].

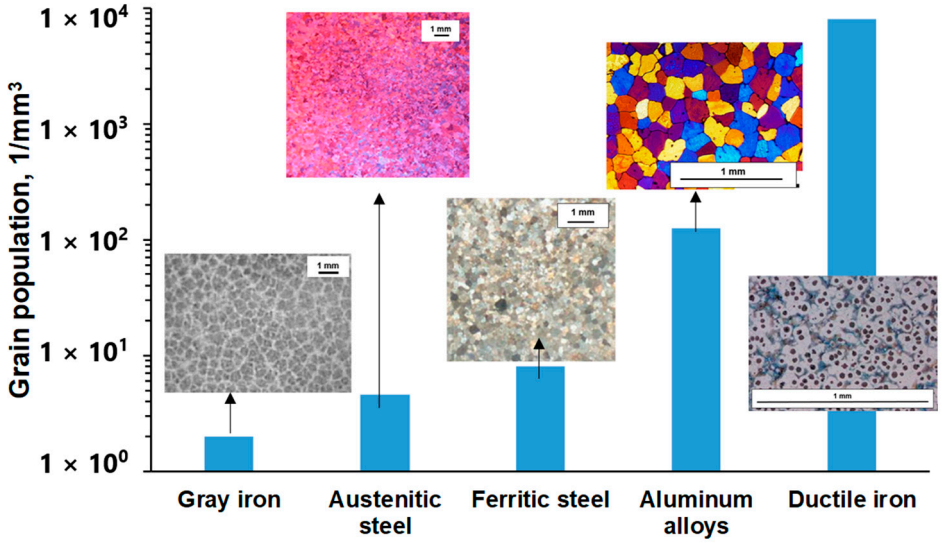


Figure 1. Volumetric grain number in the solidification structure of different cast alloys with a refined structure [3].

Homogeneous nucleation from stochastically formed nanometer-scale embryos requires a deep undercooling of the metallic melt, which is typically on the order of one hundred degrees Celsius, to overcome the energy barrier. The observed undercooling of a few degrees Celsius in commercial metallic alloys indicates heterogeneous nucleation on the existing nuclei. If the melt is in contact with a flat, relatively large solid support, compared to the homogeneous nuclei at the critical radius, then this surface will facilitate heterogeneous nucleation by decreasing the total value of Gibbs energy as a function of $f(\theta)$:

$$\Delta G_{het} = f(\theta) \cdot \Delta G_{hom} \quad (1)$$

where: ΔG_{het} is the Gibbs energy for heterogenous nucleation, ΔG_{hom} is the Gibbs energy for homogenous nucleation, and θ is a contact angle at the triple junction between the solid support, nuclei, and melt.

The real solid supports in the melt, which facilitate heterogeneous nucleation, are not infinite and ideally flat. To determine an optimal surface topology of heterogeneous nuclei, SE-FIT software was used in our study [1]. The function $f(\theta)$ was simulated for a variety of sizes and shapes of potential heterogeneous nuclei, and the results are plotted in Figure 2. It was found that decreasing the contact angle on an infinitely large, flat substrate reduced $f(\theta)$ and the needed undercooling for heterogeneous nucleation (critical undercooling). It should be noted that the effect of the contact angle also depends on the support dimension and geometry. When a nucleus with radius R sits on a small spherical substrate with radius r, decreasing the contact angle does not significantly impact $f(\theta)$ or effectively reduce the critical undercooling. It was found that a value higher than the minimal dimensional r/R ratio is needed to effectively facilitate heterogeneous nucleation. The second factor is related to the geometry of the potential nucleation site, which is typically not flat or spherical. For example, formed in the ductile iron melt complex oxide, nitrides and sulfides have irregular shapes comprising convex and concave surfaces or folded internal corners (insertion in Figure 2) [2–5]. The formation sequence of such complex inclusions during ductile iron melt treatment are described in the next parts of this article. The "folded" inclusions have a significant nucleation advantage relative to a flat support. Complex "folded" precipitates generate additional sites for continuous nucleation. The different

process routes to develop such complex heterogeneous nuclei in liquid alloys by in situ chemical reactions are discussed in the later sections.

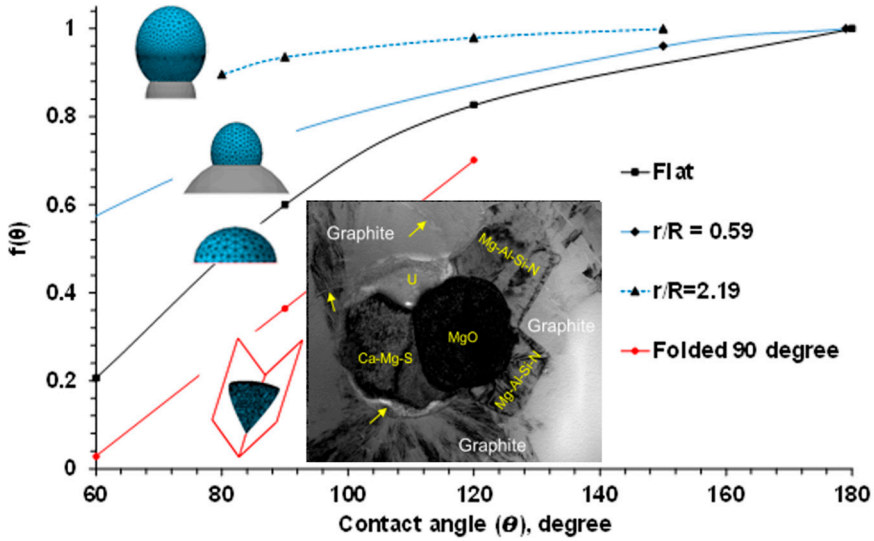


Figure 2. Effects of contact angle (θ), dimensional ratio (r/R), and shape of nuclei on the function $f(\theta)$, simulated with SE-FIT/Surface Evolver software. Inserted picture of complex nuclei is described in next part of this article.

The thermodynamic analysis of heterogeneous nucleation provides the theoretical basis for a variety of metallurgical inoculation processes that were designed using an *engineering heterogeneous nucleation* methodology.

2. Engineering Inoculation of Cast Iron with Spherical Graphite

2.1. Thermodynamic Simulation

Non-metallic inclusions play a vital role in graphite nodule nucleation for cast iron with spheroidal graphite (SGI). Because each graphite nodule needs a nucleation site, more than tens of thousands of heterogeneous nuclei per mm^3 are needed to avoid undesirable cementite formation when a liquid phase undercools below a meta-stable eutectic transformation temperature. Knowledge about the composition of heterogeneous nuclei is practically important and can be used to control solidification in SGI castings. A typical SGI metallurgical processing includes nodularization treatment by *Mg* with rare earth (*RE*) metals (*Ce*, *La*) to promote the formation of spherical graphite, followed by inoculation with *Fe*75%*Si* base inoculants containing active elements, such as *Al*, *Ca*, *Ba*, *Zr*, *Ce* and *La*. In the published results, thermodynamic simulations were performed to predict the types of non-metallic precipitates formed during the entire SGI process, including the melt nodularization and inoculation, as well as the subsequent melt cooling and casting solidification [2–9].

The thermodynamic simulations showed that the precipitates developed during SGI processing could be classified into three classes related to different formation conditions (Figure 3):

- *primary thermodynamically stable precipitates* developed in the melt during nodularization treatment with complex *Mg-RE* alloy;
- primary meta-stable precipitates formed during Fe-Si-based inoculant dissolution;

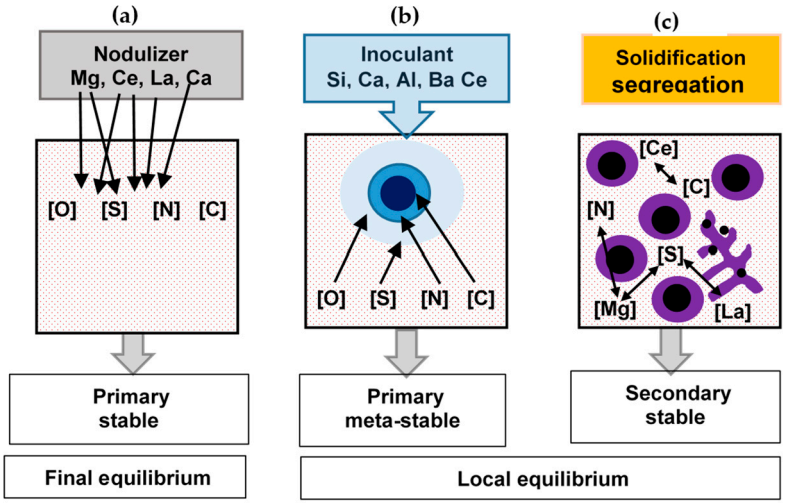
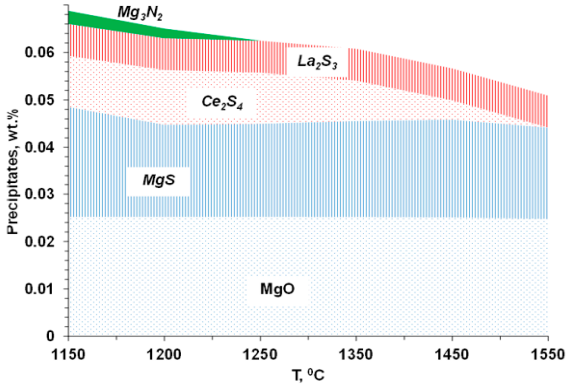


Figure 3. Methods used to simulate reactions during SGI processing: final equilibrium between elements dissolved in melt and active additions in the nodulizer (**a**), simulation of meta-stable precipitates in inoculant dissolution zones (**b**) and coupled simulation of solidification segregation and chemical reactions in the mushy zone (**c**) [3].

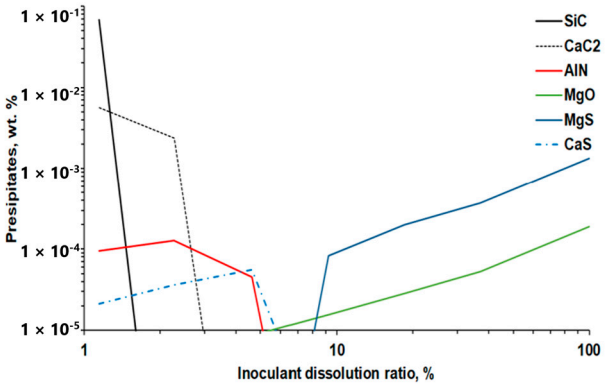
Secondary thermodynamically stable and meta-stable precipitates formed around the liquidus temperature in the mushy zone. Formation of the secondary precipitates during solidification relates to the increasing affinity of *N*, *S*, and *C* for the *Mg* and *RE* dissolved in the melt with lowering temperature, and is accelerated by the positive segregation of these elements into the remaining melt. This category of precipitates mainly includes complex *Mg-Al-Si* nitrides.

There are many competitive reactions that could occur during the nodularization treatment, and thermodynamic simulations were used to simulate the composition of specific reaction products, considering the SGI melt chemistry, the composition of additions, and changing melt temperature during SGI processing (Figure 4). The reaction products formed during the *Mg-RE* nodulizing treatment were typically thermodynamically stable in the melt (Figure 4a). Meanwhile, equilibrium simulations of the reactions during *Fe-Si*-base inoculation showed that only a few new precipitates could be formed because this treatment followed the deep melt refining of dissolved *S* and *O* during previous nodularization with *Mg*. This indicated that the equilibrium simulation could not explain the strong effect of the *Fe-Si* inoculation on increasing the graphite nodule count.

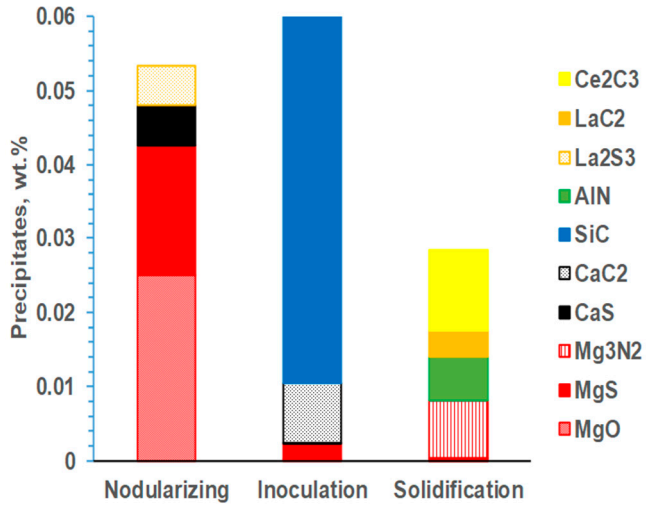
Instead, the local reactions in the melt during the *Fe-Si*-based inoculant dissolutions were estimated by dynamic imitation of the dissolution zone in the melt to understand the interactions during the inoculation process [7,8]. Assuming quick irreversible reactions in the inoculant dissolution zones, the formed reaction products were "removed" from the system after each simulation step. Accordingly, the several formed precipitates could be predicted during inoculant dissolution (Figure 4b). For example, at the initial stage of inoculant dissolution (low dissolution ratio), *SiC* and CaC_2 can be formed in the high silicon melt located close to the inoculant addition surface. It is important to note that these reaction products have a meta-stable nature and will be redissolved back into the melt during holding, which explains the fading of the inoculation over several minutes while holding the melt.



(**a**)



(**b**)



(**c**)

Figure 4. Thermodynamic prediction of inclusion family developed during melt nodularization with *Mg-Ce-La* addition (**a**), simulated meta-stable precipitates formed during *Fe-Si* base inoculant dissolution (**b**), and families of inclusions formed during entire SGI process (**c**) [3].

Finally, the precipitation of new secondary inclusions in the mushy zone is possible because of the developing segregations of the active elements in front of the austenite. The family of these secondary inclusions includes *Mg-Al-Si* or *Ti/Zr* nitrides, and the secondary precipitate composition depends on the dissolved residuals in the melt. It is important to mention that the co-precipitation of secondary precipitates on the exiting solid surfaces

resulted in multiple internal corners on the convex and concave surface. The increasing nucleation potential of such precipitate geometry was predicted from the simulations (Figure 2). The simulated precipitate families for the entire SGI process simulation are shown in Figure 4c.

2.2. Analysis of Heterogeneous Nuclei

The thermodynamic simulations predict a variety of precipitates formed during SGI processing, mold filling, and casting solidification. To verify these predictions, the automated SEM/EDX analysis of inclusion family was performed [3,6]. A procedure for separately searching for nuclei in the center of graphite nodules and located in the metal matrix was developed. To achieve reasonable statistical results, up to 10,000 nodules were searched, which gave information about several hundreds of nuclei. Examples of individual non-metallic inclusions detected inside graphite nodules on the polished cross section and electrolytically extracted from the matrix are provided in Figure 5.

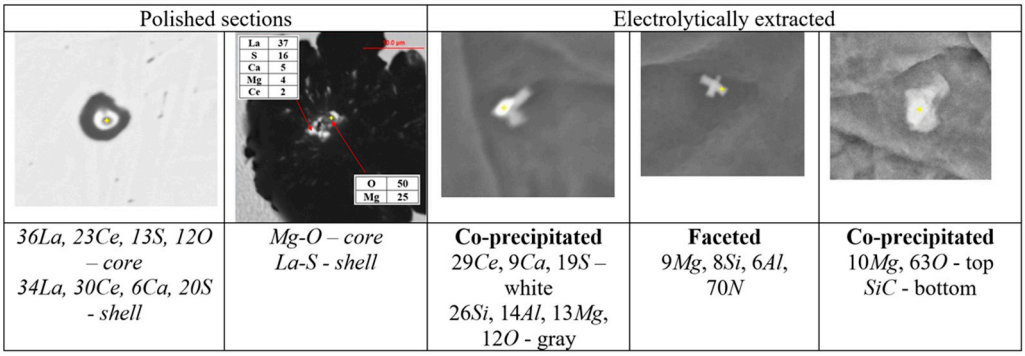


Figure 5. Examples of non-metallic inclusions detected in graphite nodules on the polished section and electrolytically extracted from SGI.

Ternary plots of classified oxides, sulfides and nitrides located in the matrix and at the center of graphite nodules are presented in Figure 6. Three classes of precipitates were detected in the metal matrix and inside the graphite nodules: complex *Mg-Al-Si* nitrides, complex *Al-Si-Mg* and *Mg-Ce-La* oxides, and *Mg-Ca* and *La-Ce* sulfides. These types of reaction products in the melt were predicted by the thermodynamic simulations (Figure 4). The studied ductile iron contained a limited amount of other nitride-forming elements (*Ti* and *Zr*); therefore, only the complex *Mg-Al-Si* nitrides were detected in this case.

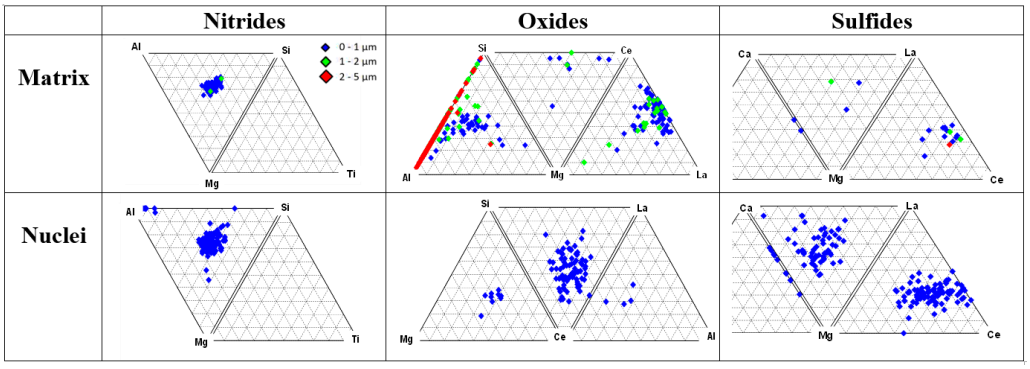


Figure 6. Ternary plots of non-metallic inclusion families (nitrides, oxides, and sulfides) detected in matrix and inside graphite nodules [3].

The results of the automated SEM/EDX analysis of non-metallic inclusions in the industrial and laboratory-melted SGI were described in [3–7]. An example demonstrating a significant difference in the composition of non-metallic inclusion located in the metal matrix versus inside graphite nodules can be observed in the ternary diagrams in Figure 6.

To quantify these differences, the average concentrations of active elements and their partitioning into those situated inside the graphite nodules against the matrix were calculated for all the detected inclusions (Figure 7). *Ti* had a large negative value of partitioning and was situated mainly in the matrix, while *Ca* and *La* sulfides had tendency to present in the graphite nuclei. The graphite nuclei contained significantly larger portions of *La* and *Ca* sulfides and *Zr* nitrides, which indicates their nucleation activity. Such an analysis could be used to optimize the inoculation practice.

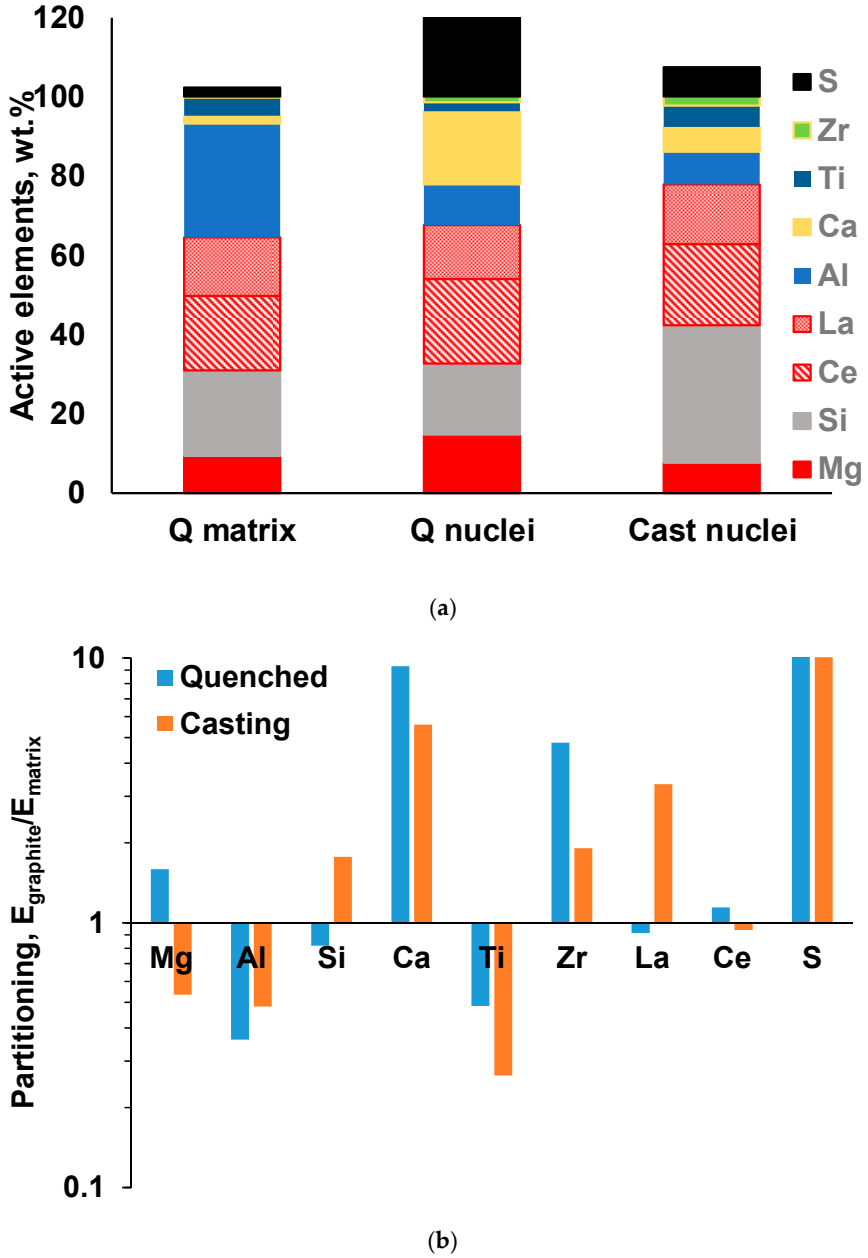


Figure 7. Average composition of active elements (note that S is plotted above 100%) (**a**) and partitioning coefficients of active elements between nuclei and matrix in quenched and cast SGI (**b**) [3].

The authors [7] conducted detailed atomic-resolution TEM (transmission electron microscopy) analysis of the interface between the complex heterogeneous nuclei and the graphite nodule and discovered evidence of meta-stable reaction products, which could have formed during the inoculation process (Figure 8).

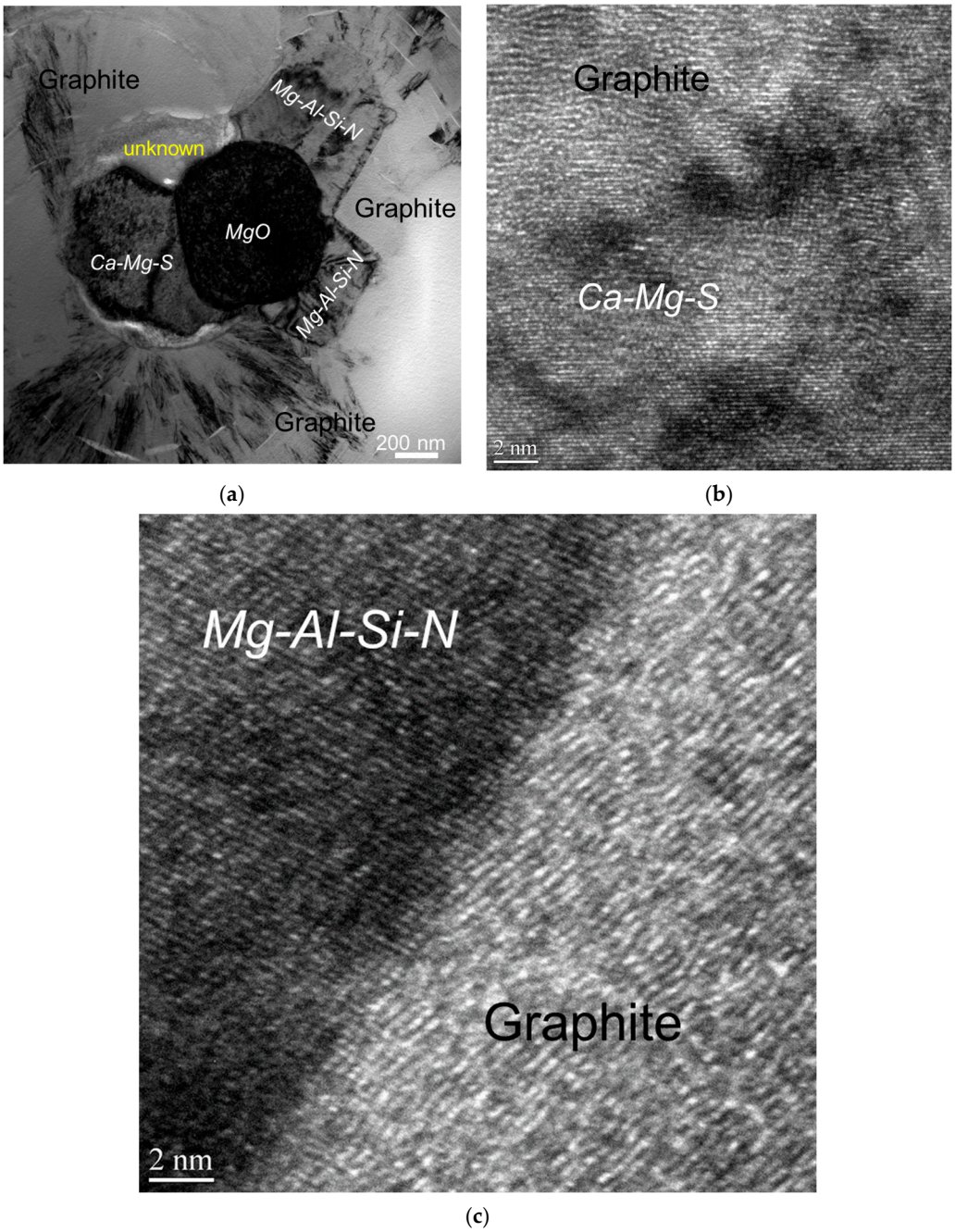
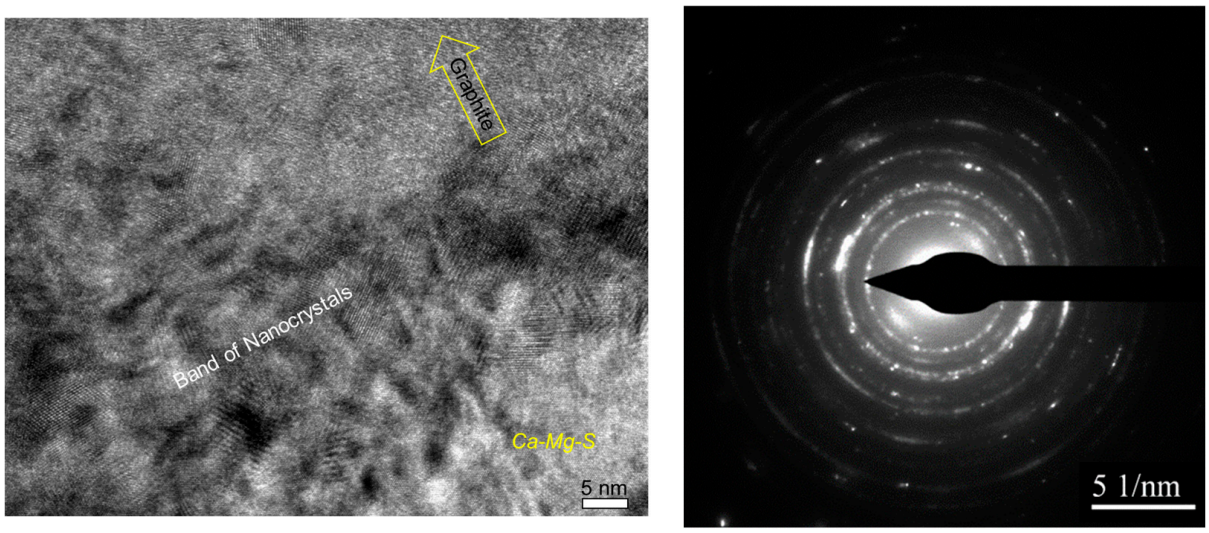


Figure 8. Bright-field TEM image showing complex heterogeneous nuclei of a graphite nodule (**a**) and the atomic-resolution TEM images of interfaces between graphite and nuclei compounds (**b**,**c**) [7].

The nanocrystal band, which was located between the complex precipitates and graphite nodule (Figure 9), can be the product of transient reactions during the inoculation process with *Fe-Si* addition (Figure 4). The atomically rough interface of the nanocrystalline band is highly active in the initialization of graphite nucleation because it contains plenty of sharp, concave regions and provides greater surface areas.



(**a**) (**b**)

Figure 9. Nanocrystal band on graphite/nuclei interface: (**a**) high-resolution TEM image and (**b**) selected area diffraction pattern [7].

2.3. Control Solidification Kinetics for Self-Healing Microporosity in SGI

Thermodynamic simulations and an experimental searching methodology of graphite nodule nuclei were used for the optimization of SGI processing, and the term engineering of non-metallic inclusions in SGI for controlling graphite nodule nucleation is suggested by the author to describe this methodology [2]. The SGI melt treatment optimization was motivated by the development of the following goals:

- *types of non-metallic inclusions* to initiate heterogeneous nucleation of graphite nodules;
- *topology of these precipitates* (dimension, number, and shape) to become active nuclei;
- *sequence of precipitate formation* for prolongation of nucleation events until the end of solidification.

Practical applications of the engineering of non-metallic inclusions in SGI to control graphite nodule nucleation were described by the author with colleagues and students in the articles related to reducing shrinkage microporosity in casting [2,9–14]. Graphite precipitation from the melt causes volume expansion during solidification; therefore, the control of the kinetics of graphite nodule precipitation could be used as an effective way to eliminate shrinkage microporosity. Let us consider two solidification scenarios: (i) instantaneous graphite nodule nucleation at maximal undercooling and (ii) continuous graphite nodule nucleation toward the end of solidification. In the first solidification scenario, the volume increase, caused by massive graphite growth during the early solidification stage, will provide pressure on the mold/casting interface, and the soft casting surface could swell when the casting is contained in the non-rigid mold. The following reduction of melt volume upon cooling will be not compensated because the developed solid network blockades direct the feeding of isolated melt pockets, and microporosity will be formed (Figure 10a). The second scenario assumes the transient continuous nucleation and growth of graphite nodules until the end of solidification. This scenario will decrease microporosity (Figure 10b). In the ideal case, the latter solidification mode could provide self-healing shrinkage in the castings solidified without risers. The technical possibility of self-healing shrinkage by the combination of intrinsic factors (effective melt inoculation) with extrinsic factors (increasing mold rigidity) was experimentally confirmed in SGI.

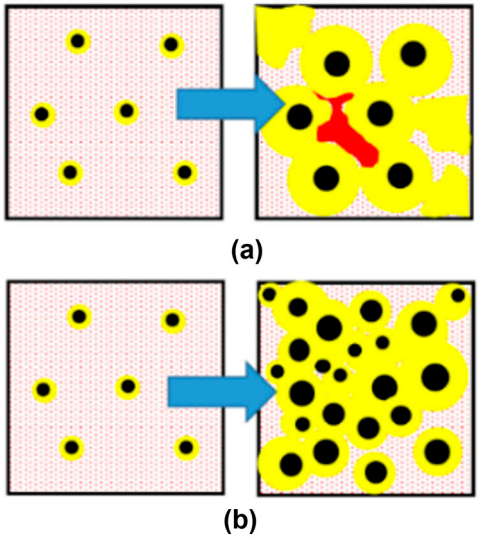


Figure 10. Two possible scenarios of graphite nodule nucleation kinetics: (**a**) instantaneous nucleation at solidification initiation (at maximum undercooling) with microporosity formation (red) and (**b**) a combination of instantaneous and continuous nucleation toward the end of solidification, which enhances self-healing microporosity in SGI.

To verify this assumption, two experimental SGIs with different intensities of heterogeneous nucleation were intentionally produced by varying the inoculation parameters [10]: SGI #1 was inoculated with foundry-grade *Fe*75%*Si* and poured at a high temperature (1400 °C), and SGI #2 was treated by *Ce*-bearing (slower fading rate) inoculant and poured at a low temperature (1320 °C). To induce microporosity formation, the riser-less test designs consisted of a horizontal plate with top vertical cylinders, where microporosity was expected and was evaluated using density measurement and microcomputed tomography (μ-CT) scanning. The 3D-morphological characteristics of the graphite nodules were determined by μCT scanning, and the obtained statistical data are discussed with respect to graphite nodule nucleation mode and casting soundness. It was shown that the 3D nodule diameter distributions were not monotonic in either inoculated SGI. A set of large nodules coexisted with sets of medium and small particles. However, well-inoculated SGI#2 treated by the *Ce*-bearing inoculant had a significantly higher graphite nodule volume number and a larger portion of small nodules when compared to SGI#1 treated by foundry-grade ferrosilicon inoculant (Figure 11).

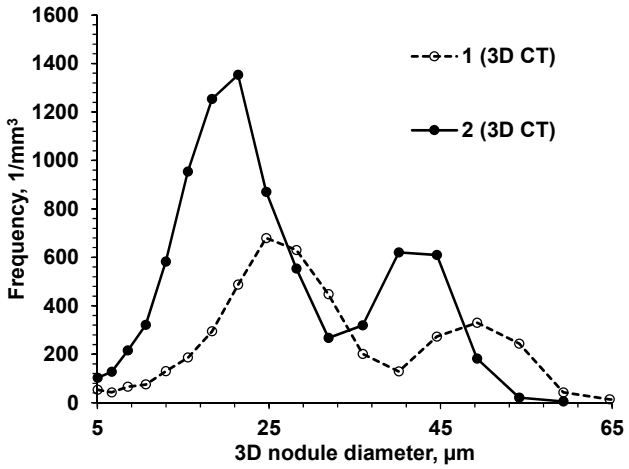


Figure 11. 3D nodule diameter distribution obtained from μCT data for two SGIs [10].

A visual presentation of graphite nodule distributions by diameter in three even groups is given in Figure 12a,b for both SGIs. A color code was applied: blue for large and red for small nodules, while medium nodules were removed to better visualize the clustering of small nodules in the interdendritic regions where cast iron solidified at the end. The 3D analysis showed a significantly lower level of microporosity in SGI#2 (red highlights in Figure 12c,d). The effective inoculation with *Ce*-bearing inoculant at the lower temperature of SGI #2 provided a higher volume nodule number and a well-defined bi-modal nodule diameter distribution with larger portions of small- and medium-diameter nodules. The space distribution pattern of graphite nodules and bi-modal diameter distribution indicate that the effective inoculation promoted continuous nucleation towards the end of solidification in addition to the early wave of graphite nucleation. Therefore, the control of the graphite nodule nucleation mode by the effective melt inoculation can be used to promote multi-wave nucleation throughout solidification and to decrease the propensity for microshrinkage.

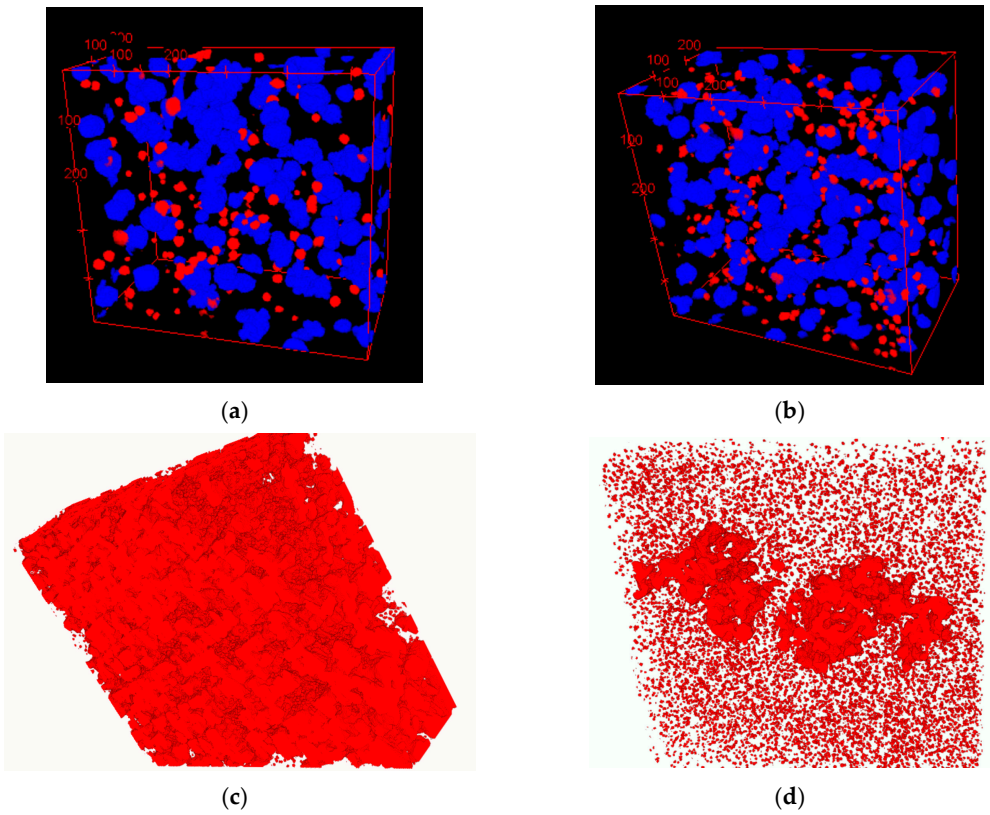
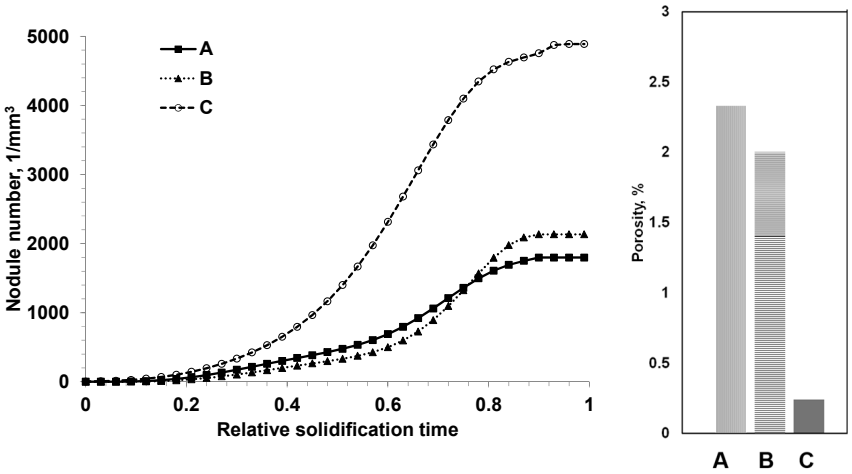


Figure 12. 3D distribution of large (blue) and small (red) graphite nodules (**a**,**b**) and rendered microporosity (**c**,**d**) in SGI#1 (**a**) and SGI#2 [10].

These results showed a practical application of engineering heterogeneous nucleation for control solidification kinetics and structure in SGI; therefore, a novel method for the structural reconstruction of solidification kinetics in cast iron with spherical graphite (SGI) was suggested by the author [13]. The ideal spherical shape of graphite nodules and the assumptions that the nodule nucleation rate $n = dN/d\tau = f(\tau)$ and the growth velocity $V = dR/d\tau = \psi(\tau)$ are time (τ)-dependent functions were used in the numerical integrator to simulate an arbitrary graphite nodule diameter distribution. This simulated distribution was fitted to the real experimental 3D graphite nodule distribution using an inverse simulation program by minimizing the error function. The obtained nucleation $f(\tau)$ and growth $\psi(\tau)$ functions showed that the solidification kinetics develop similarly to the observed experimental 3D nodule diameter distribution. The experimental structure parameters were obtained from μCT analysis [10] or by converting the experimental 2D

distribution from the polished section to the virtual 3D using the method suggested by the authors [15–17].

The structural reconstruction of solidification kinetics from the experimentally observed 3D distribution of graphite nodules was used to determine how graphite nodules were developed in the real castings and to visualize the effects of cooling rate and inoculation [13]. It was shown that the SGI solidification kinetics in the industrial castings significantly differed from those predicted by the basic instantaneous nucleation models. The cooling rate and inoculation had large impacts on the kinetics of graphite nodule nuclei formation during solidification. Figure 13 presents the kinetics of nodule number development during solidification in three SDI castings produced with different inoculation parameters and measured microporosity [14]. It was proved that the observed bi-modal distribution of nodule size in the well-inoculated SGI was related to the second nucleation wave. The suggested method provides insight into the nucleation process in SGI casting and can be used as a tool for process control, for example, with self-healing microporosity.



(**a**) (**b**)

Figure 13. Reconstructed solidification kinetics from observed microstructure in three castings obtained with different inoculation parameters (**a**) and experimentally measured porosities (**b**) [14].

The control of heterogeneous nucleation in combination with alloying by *Si*, *Al* and *Mo* were used to improve the high-temperature performance of SGI [18–24]. Additional melt treatment was used for the development of a dual graphite structure with controlled zones from the flake and spherical graphite shapes in one casting [25,26]. Practical methods to improve SGI inoculation techniques were discussed in [27,28]

3. Effect of Heterogeneous Nucleation on Shape of Primary Faceted Phases in Alloys

In previously discussed cases, engineering heterogeneous nucleation was used to control the microstructure of cast iron with spherical graphite. In this part of the overview, the authors would like to demonstrate that efficient nucleation can also be used to control the shape of primary precipitates formed directly from the melt in multicomponent hyper-eutectic alloys. In recent years, such alloys have been considered multifunctional, providing unique properties such as wear and creep resistances. The main challenge for the production of hyper-eutectic compositions is related to the tendency to form large, faceted dendrite/star-type primary phases because they are free-growing in the melt without restrictions.

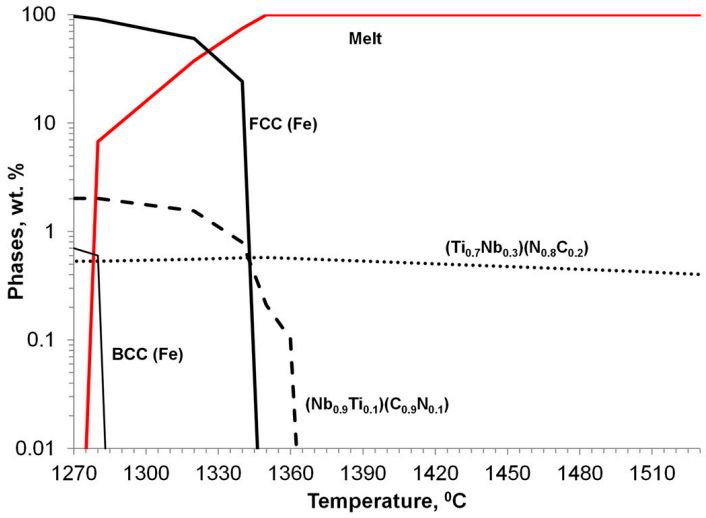
The small crystals nucleated in the melt have a compact shape near equilibrium, which can be predicted by Gibbs–Curie–Wullf's theorem that relates crystal shape to the anisotropy of surface energy. However, the following instabilities of freely growing interfaces produce morphological shape evolution. The factors that lead to shape instability include: (i) surface energy of a curved interface, (ii) atom attachment kinetics, (iii) trap-

ping solute elements, (iv) mass transport of alloying elements, and finally, (v) possible constrained growth in the liquid channels at the end of solidification. Because of these disturbances, the solidified crystal begins to develop a complex dendritic shape, growing in a kinetically but not thermodynamically preferred crystallographic direction. Consequently, at the low anisotropy of the solid–liquid interfacial energy in metallic phases, the developed non-faceted dendrites exhibit a large tip radius, while covalent and ionic phases at the high anisotropy of the solid–liquid interfacial energy exhibit a sharp, faceted morphology.

Two practical methods can be used to improve the shape of primary phases in casting from hyper-eutectic alloys: increasing the cooling rate and effective nucleation. The two methods work differently but yield similar results by minimizing the dimensions of the melt envelop around the individual crystal, which limits turbulence during crystal growth. Engineering tools could be used to control the shape of primary phases, and several examples are described below [29,30].

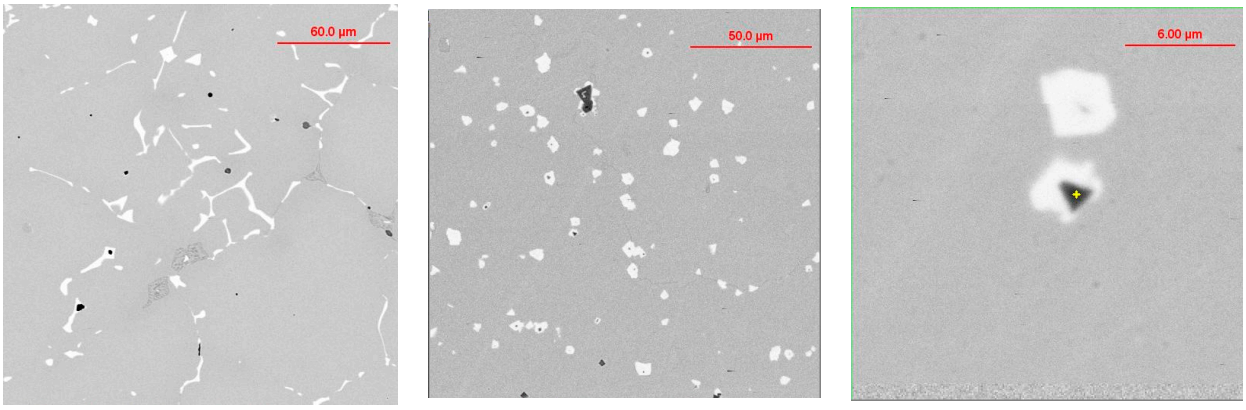
3.1. Modification of Shape of Primary Nb Carbo-Nitrides in 20%Cr, 15%Ni, 2%Nb Austenitic Steel

Niobium alloying is used to prevent creep in *Cr/Ni* alloying austenitic steel; however, primary *Nb* carbonitrides form a network of faceted, plate-like precipitates located at the grain boundary, which negatively impacts the steel's ductility (Figure 14b). A simulated sequence of primary *Nb* carbonitride formation above the austenite liquidus temperature is shown in Figure 14a. The thermodynamic simulation demonstrated the possibility of the heterogeneous nucleation of primary *Nb*-based carbonitrides by the early precipitation of *Ti*-based nitrides. The co-precipitation of *Nb*-based carbonitride changes from a plate-like topology to compact, faceted, and isolated crystals (Figure 14c). The EDX analysis (Figure 14d) revealed the composition of *Ti*-based nitrides inside co-precipitated *Nb*-based carbonitrides. A TEM sample was prepared using the focused ion beam to examine the interface between these phases. The boundary between the two phases appeared relatively flat at a high magnification using TEM (Figure 15a), EDX line scan was used for phase identification (Figure 15b), and selective area electron diffraction indicated that the *Nb*-based and *Ti*-based compounds were mostly epitaxial.



(**a**)

Figure 14. *Cont.*



(**b**) (**c**) (**d**)

Figure 14. Thermodynamic simulation of solidification sequence in *Ti*-modified *Nb*-alloyed *Cr-Ni* austenitic steel (**a**); SEM images of base/unmodified (**b**) and modified (**c**,**d**: black 44%*Ti*, 20%*Nb*; white 40%*Nb*, 18%*Ti*) steels.

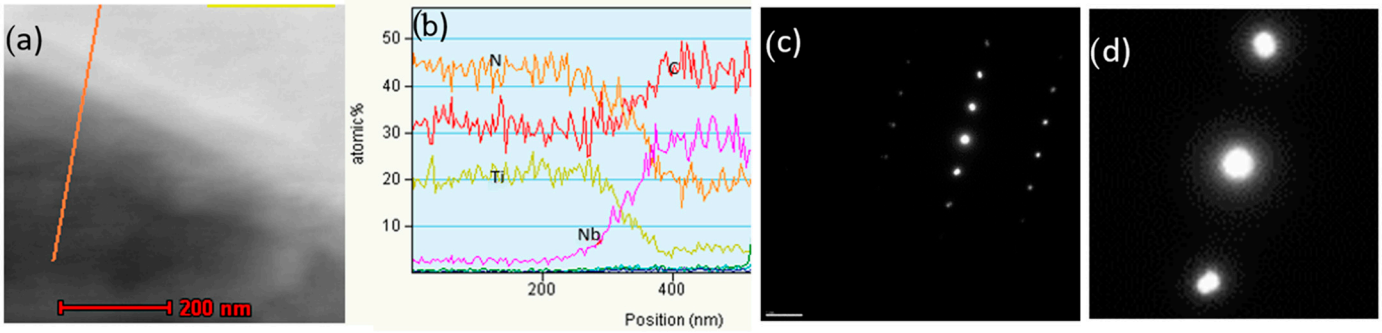
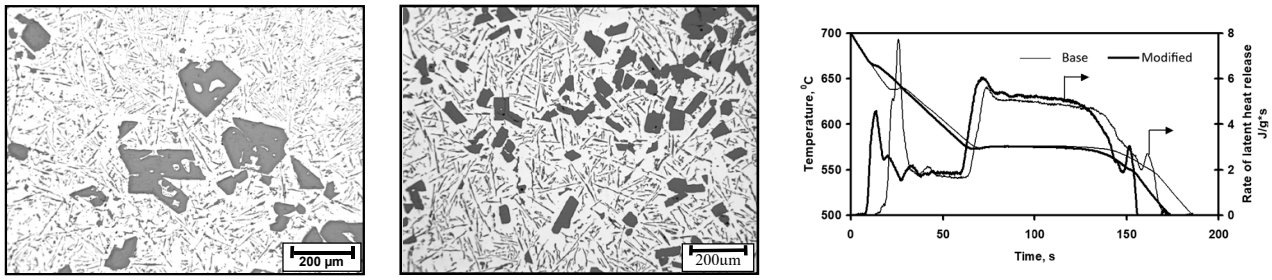


Figure 15. TEM STEM bright-field image of boundary between *Ti*-based (dark) and *Nb*-based (bright) phases with the scanning line (**a**), EDX line scan result (**b**), and electron diffraction pattern from overlapped boundary between two phases (**c**,**d**).

3.2. Modification of Shape of Primary Covalent Phases in Hyper-Eutectic Non-Ferrous Alloys

The shape modification of the primary covalent phases (*Si*, Mg_2Si and *Al-Sb*) in several *Al*- and *Mg*-based hyper-eutectic alloys was investigated [29,30]. These types of alloys have been recently discussed for different friction-, wear-, and creep-resistant applications. They contain primary phases with a covalent atomic bond: for example, *Si* crystals in *Al*-18%*Si* alloy, *Al-Sb* crystals in *Al*–5.5% *Sb* alloy, or Mg_2Si in hyper-eutectic *Al-Mg-Si* and *Mg-Si* alloys. All these phases have irregular star- and plate-like faceted shapes in casting (Figures 16a and 17a).



(**a**) (**b**) (**c**)

Figure 16. Microstructures of aluminum alloys with 18% Si: (**a**) base case and (**b**) modified by 0.05% P, and (**c**) thermal analysis of both alloys.

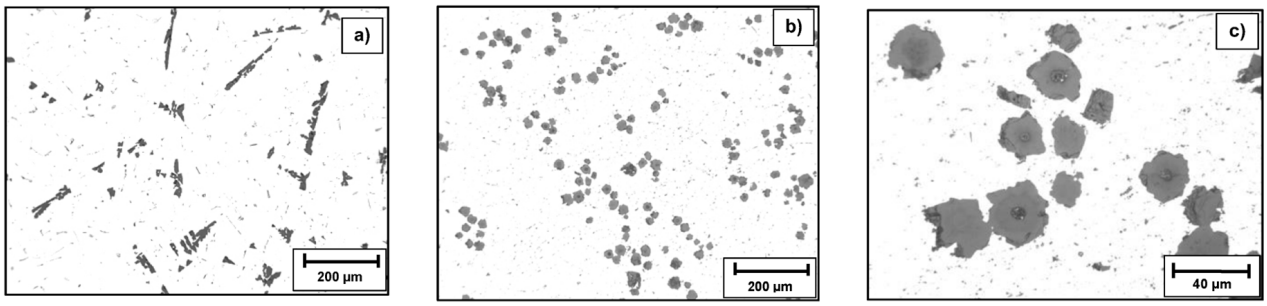


Figure 17. Microstructures of Al–5.5% Sb alloy: (**a**) base and (**b**,**c**) modified by 0.5% Te.

The design of additions for the shape modification of the primary covalent, faceted crystals was conducted from the analysis of its in situ capability to form heterogeneous nuclei in the melt at the optimal temperature window above the liquidus temperature. Typically, inoculants were taken from the next group of elements in periodic system, for example, *P* for *Al-Si*, *Al-Mg-Si* and *Mg-Si* alloys and *Se* or *Te* for *Al-Sb* alloy. The thermodynamic simulation predicted the in situ formation of heterogeneous nuclei such as *AlP* in *Al-Si* alloy. In *Al*-18%*Si* alloy, the addition of 0.05% *P* increased the number of primary *Si*-crystals and decreased their average size by 3–4 times (Figure 16b), and the shape of the primary *Si* crystals was converted to compact rectangular with faceted planes. The thermal analysis indicated the increasing liquidus temperature and decreasing undercooling of primary *Si* phase after promoted heterogeneous nucleation with fine *AlP* precipitates.

Modification provided a similar shape modification in the other mentioned hyper-eutectic alloys. Figure 17 illustrates the shape changes in hyper-eutectic *Al-Sb* alloy treated by 0.5% *Te*. The cores of the primary *Al-Sb* intermetallic phase in the modified alloy contained the complex heterogeneous nuclei that were formed in situ and attributed to the reaction of the *Te* additions with the alloy components.

4. Conclusions

This overview aims to summarize the published studies by the authors in co-authorship with colleagues and students on different aspects of engineering heterogeneous nucleation in solidified cast alloys with a multiphase structure formed during solidification. The engineering heterogeneous nucleation has a unique possibility to modify the cast structure in the desired direction to improve casting quality. The described thermodynamic simulations and experimental tools were used to design process parameters and the provided methodology is applicable for engineering heterogeneous nucleation in different alloys. The several steps for engineering heterogeneous nucleation included the design of active additions, optimization of topology of heterogenous nuclei, thermodynamic simulation of process parameters, and a set of experimental methods such as an automated SEM/EDX analysis of precipitate family. Such a methodology was used as a practical tool for inducing self-healing microporosity in SGI by enhancing heterogeneous nucleation. This overview briefly provided practical details of the mentioned processes, and a full description can be found in the referred articles. The author appreciates the great efforts that the co-authors have made on the original articles that were overviewed here.

Author Contributions: S.N.L.—conceptualization, data gathering, writing—original draft preparation; J.Q.—visualization and review. All authors have read and agreed to the published version of the manuscript.

Funding: This research received no external funding.

Data Availability Statement: The data presented in this study are available on request from the corresponding author.

Acknowledgments: The author gradually thanks all coauthors of overviewed articles. The mentioned studies were done at Metal Casting Laboratories at Missouri University of Science and Technology and Georgia Southern University and supported by American Foundry Society and Ductile Iron Society. The authors very appreciate their long-term support.

Conflicts of Interest: The authors declare no conflict of interest.

References

1. Arvola, D.; Lekakh, S.; O'Malley, R.; Bartlett, L. Two Inoculation Methods for Refining As-Cast Grain Structure in Austenitic 316L Steel. *Int. J. Met.* **2019**, *13*, 504–518. [CrossRef]
2. Lekakh, S. Engineering Nucleation Kinetics of Graphite Nodules in Inoculated Cast Iron for Reducing Porosity. *Met. Mater. Trans. B* **2018**, *50B*, 890–902. [CrossRef]
3. Lekakh, S. Searching for Graphite Nodule Nuclei Using Automated SEM/EDX Analysis. *Int. J. Met.* **2020**, *14*, 1078–1089. [CrossRef]
4. Lekakh, S.; Richards, V.; Peaslee, K. Thermo-chemistry of Non-metallic Inclusions in DI. *Int. J. Met.* **2009**, *4*, 25–37.
5. Lekakh, S.; Robertson, D.; Loper, C. Thermochemistry and Kinetics of Iron Melt Treatment. In Proceedings of the World Foundry Congress, Harrogate, UK, 5–7 June 2006.
6. Lekakh, S. Effect of Non-metallic Inclusions on Solidification of Inoculated Spheroidal Graphite Iron. *Int. J. Met.* **2019**, *1*, 47–57.
7. Qing, J.; Lekakh, S.; Xu, M.; Field, D. Formation of Complex Nuclei in Graphite Nodules of Cast Iron. *Carbon* **2021**, *171*, 276–288. [CrossRef]
8. S Lekakh, S.; Loper, C. Improving inoculation of ductile iron. *AFS Trans.* **2013**, *111*, 885–894.
9. Loper, C.; Lekakh, S. Additive for Inoculation of Cast Iron and Method. U.S. Patent 7,081,150, 25 July 2006.
10. Lekakh, S.N.; Zhang, X.; Tucker, W.; Lee, H.K.; Selly, T.; Schiffbauer, J.D. 3D Characterization of Structure and Micro-porosity in Two Cast Irons with Spheroidal Graphite. *Mater. Charact.* **2019**, *158*, 109991. [CrossRef]
11. Lekakh, S.N.; Zhang, X.; Tucker, W.; Lee, H.K.; Selly, T.; Schiffbauer, J.D. Micro-CT Quantitative Evaluation of Graphite Nodules in SGI. *Int. J. Met.* **2020**, *14*, 318–327. [CrossRef]
12. Lekakh., S.; Khayat, M. Effects of Metallurgical Factors on Micro-porosity in Ductile Iron, AFS. In Proceedings of the 123rd Metalcasting Congress, Atlanta, GA, USA, 27–30 April 2019; pp. 19–157.
13. Lekakh, S. Structural Reconstruction of Solidification Kinetics in Cast Iron with Spherical Graphite. *ISIJ Int.* **2016**, *56*, 812–818. [CrossRef]
14. Lekakh, S.; Hrebec, B. Solidification Kinetics of Graphite Nodules in Cast Iron and Shrinkage Porosity. *Int. J. Met.* **2016**, *10*, 389–400. [CrossRef]
15. Lekakh, S.; Qing, J.; Richards, V.; Peaslee, K. Graphite Nodule Size Distribution in Ductile Iron. *AFS Proc.* **2013**, 1313–1321.
16. Lekakh, S.; Harris, M. Novel Approaches to Analyze the Structure of Ductile Iron. *Int. J. Met.* **2014**, *8*, 41–49. [CrossRef]
17. Lekakh, S. Communication: Characterization of Spatial Distribution of Graphite Nodules in Cast Iron. *Int. J. Met.* **2017**, *11*, 743–748. [CrossRef]
18. Lekakh, S.N.; Athavale, V.A.; Bartlett, L.; Godlewski, L.; Li, M. Effect of Micro-structural Dispersity of SiMo Ductile Iron on Thermal Cycling Performance. *Int. J. Met.* **2022**. [CrossRef]
19. Lekakh, S.N.; Bofah, A.; Godlewski, L.A.; Li, M. Effect of Micro-Structural Dispersity of SiMo Ductile Iron on High Temperature Performance during Static Oxidation. *Metals* **2022**, *12*, 661. [CrossRef]
20. Lekakh, S.N.; Johnson, C.; Godlewski, L.; Li, M. Control of High-temperature Static and Transient Thermomechanical Behavior of SiMo Ductile Iron by Al Alloying. *Int. J. Met.* **2023**, *17*, 22–38. [CrossRef]
21. Lekakh, S.N.; Bofah, A.; Osei, R.; O'Malley, R.; Godlewski, L.; Li, M. High Temperature Oxidation and Decarburization of SiMo Cast Iron in Air and Combustion Atmospheres. *Oxid. Met.* **2021**, *95*, 251–258. [CrossRef]
22. Lekakh, S.N.; Buchely, M.; O'Malley, R.; Godlewski, L.; Li, M. Thermo-cycling Fatigue of SiMo Ductile Iron using a Novel Thermo-Mechanical Test. *Int. J. Fatigue* **2021**, *148*, 106218. [CrossRef]
23. Lekakh, S.N.; Bofah, A.; Chen, W.T.; Godlewski, L.; Li, M. Prevention of High-Temperature Surface Degradation in SiMo Cast Irons by Cr and Al Alloying. *Met. Mater. Trans. B* **2020**, *51B*, 2542–2554. [CrossRef]
24. Lekakh, S.N.; Tucker, W.; Bofah, A.; Selly, T.; Godlewski, T.; Li, M. Quantitative μ-CT Analysis of Scale Topology Formed During Oxidation of High SiMo Cast Iron. *Oxid. Met.* **2020**, *94*, 251–264. [CrossRef]
25. Qing, J.; Lekakh, S.; Richards, V. No-bake S-containing Mold-DI Metal interactions: Consequences and Potential Application. *Trans. Am. Foundry Soc.* **2013**, *13*, 1320.
26. Qing, J.; Lekakh, S.; Richards, V. Investigation of Cast Iron Processing to Produce Controlled Dual Graphite Structure in Castings. *Trans. Am. Foundry Soc.* **2012**, *120*, 297.
27. Lekakh, S.; Bestuzhev, N. *Ladle Metallurgy of High Quality Cast Iron*; Nauka&Tekhnika: Minsk, Belarus, 1992.
28. Lekakh, S.; Shainert, V. Methods of Improving of Cast Iron Inoculation Effectiveness. *Foundry Prod.* **1994**, *9*, 4.

29. Khudokormov, D.; Galushko, A.; Lekakh, S. Modification of Shape of Fe-containing Phases in Aluminum alloys. *Foundry Prod. USSR* **1975**, *5*, 18.
30. Khudokormov, D.; Galushko, A.; Lekakh, S. Formation of Magnesium Silicide and Fe-containing Phases in Aluminum and Magnesium Alloys. *Foundry Prod. USSR* **1973**, *3*, 25.

Disclaimer/Publisher's Note: The statements, opinions and data contained in all publications are solely those of the individual author(s) and contributor(s) and not of MDPI and/or the editor(s). MDPI and/or the editor(s) disclaim responsibility for any injury to people or property resulting from any ideas, methods, instructions or products referred to in the content.